A comparative study of cellulose nanofibrils disintegrated via multiple processing approaches

ARTICLE *in* CARBOHYDRATE POLYMERS · MARCH 2013

Impact Factor: 4.07 · DOI: 10.1016/j.carbpol.2013.04.086 · Source: PubMed

6 AUTHORS, INCLUDING:

Ronald Sabo
US Forest Service
37 PUBLICATIONS **266** CITATIONS
SEE PROFILE

J.Y. Zhu
US Forest Service
242 PUBLICATIONS **3,892** CITATIONS
SEE PROFILE

Umesh Agarwal
US Forest Service
110 PUBLICATIONS **1,497** CITATIONS
SEE PROFILE

Zhiyong Cai
US Forest Service
111 PUBLICATIONS **615** CITATIONS
SEE PROFILE

Carbohydrate Polymers 97 (2013) 226–234

Contents lists available at SciVerse ScienceDirect

Carbohydrate Polymers

journal homepage: www.elsevier.com/locate/carbpol

A comparative study of cellulose nanofibrils disintegrated via multiple processing approaches

Yan Qing[a,b], Ronald Sabo[b,*], J.Y. Zhu[b], Umesh Agarwal[b], Zhiyong Cai[b], Yiqiang Wu[a,**]

[a] School of Materials Science and Engineering, Central South University of Forestry and Technology, Changsha, Hunan 410004, China
[b] USDA Forest Service, Forest Products Laboratory, Madison, WI 53726-2398, USA

ARTICLE INFO

Article history:
Received 27 February 2013
Received in revised form 12 April 2013
Accepted 27 April 2013
Available online 4 May 2013

Keywords:
Cellulose nanofibrils
Refining
Microfluidization
Enzymatic and chemical pretreatments

ABSTRACT

Various cellulose nanofibrils (CNFs) created by refining and microfluidization, in combination with enzymatic or 2,2,6,6-tetramethylpiperidine-1-oxyl (TEMPO) oxidized pretreatment were compared. The morphological properties, degree of polymerization, and crystallinity for the obtained nanofibrils, as well as physical and mechanical properties of the corresponding films were evaluated. Compared to refining, intense microfluidization contributed greater separation of nanofibril bundles, which led to an enhancement of mechanical strength and transparency for the resultant film. The selected enzymatic pre-treatments produced shortened fibers due to preferential hydrolysis of amorphous cellulose and, in combination with mechanical treatments, resulted in short and stiff cellulose nanocrystal (CNC)-like materials. Despite films from these CNC-like fibrils having inferior tensile strength, their tensile modulus and transparency were significantly improved compared to CNFs prepared without pre-treatment. The unique fiber morphology and high crystallinity potentially offer a green and ecologically friendly alternative for the preparation of CNCs and CNFs as part of an integrated biorefinery approach.

Published by Elsevier Ltd.

1. Introduction

Because of its abundance and sustainability, plant cellulose and cellulosic nanomaterials have attracted growing interest as an alternative to synthetic materials, especially as a filler and reinforcement for composites. Cellulose nanofibrils (CNFs), the class of cellulosic nanomaterials examined in this work, have a diverse range of reported applications including paper additives (Sehaqui, Allais, Zhou, & Berglund, 2011), barrier packaging (Aulin, Gällstedt, & Lindström, 2010), pharmaceutical carrier (Czaja, Young, Kawecki, & Brown, 2007), reinforcements for polymer composites (Qing, Sabo, Wu, & Cai, 2012; Qing, Sabo, Cai, & Wu, 2013; Srithep, Turng, Sabo, & Clemons, 2012; Tingaut, Zimmermann, & Lopez-Suevos, 2010), conductive nanopaper (Nyström et al., 2010), electronic substrates (Okahisa, Yoshida, Miyaguchi, & Yano, 2009; Sabo, Seo, & Ma, 2012), and multi-functional magnetic materials (Olsson et al., 2010). However, efficient production of cellulose nanofibril is still challenging with respect to energy consumption, commercial scale, and high capacity.

Numerous methods for creating cellulose nanofibrils have been reported since early studies (Herrick, Casebier, Hamilton, & Sandberg, 1983; Turbak, Snyder, & Sandberg, 1983), but nearly all involve some type of chemical or enzymatic pre-treatment of the plant fibers followed by intensive mechanical disintegration. Various types of mechanical operations have been applied to produce cellulose nanofibrils including homogenization (Herrick et al., 1983; Nakagaito & Yano, 2004; Stelte & Sanadi, 2009; Turbak et al., 1983), ultrafine grinding or refining (Stelte & Sanadi, 2009; Wang, Zhu, Gleisner, et al., 2012), microfluidization (Spence, Venditti, Rojas, Habibi, & Pawlak, 2011; Zhu, Sabo, & Luo, 2011; Zimmermann, Bordeanu, & Sturb, 2010), intense ultrasonication (Chen et al., 2011; Cheng, Wang, & Rials, 2009; Tonoli et al., 2012), cryocrushing in liquid nitrogen (Alemdar & Sain, 2008; Chakraborty, Sain, & Kortschot, 2005; Wang & Sain, 2007), and high-speed blending (Uetani & Yano, 2011). Due to different shear mechanisms and intensity, the energy requirement and morphologies of obtained nanofibers also vary widely. For instance, grinding or refining is considered more effective in removing external layers of the cell wall through abrasive actions, which promotes the thicker secondary cell wall to efficient fibrillation (Iwamoto, Nakagaito, & Yano, 2007; Stelte & Sanadi, 2009). Microfluidization provides significantly higher shear than others (Microfluidics Corporation, 2012), and is able to create high-performance nanofibrils (Spence et al., 2011). However, depending on the flexibility of raw material and pretreatment, fiber suspensions sometimes clog in the reaction chamber during high-pressure microfluidization (Henriksson, Henriksson, Berglund, & Lindström, 2007; Spence et al., 2011; Stelte & Sanadi, 2009).

* Corresponding author. Tel.: +1 608 231 9530; fax: +1 608 231 9582.
** Corresponding author. Tel.: +86 731 85623301; fax: +86 731 85623301.
E-mail addresses: rsabo@fs.fed.us (R. Sabo), wuyiqiang@csuft.edu.cn (Y. Wu).

0144-8617/$ – see front matter. Published by Elsevier Ltd.
http://dx.doi.org/10.1016/j.carbpol.2013.04.086

Various chemical (Saito & Isogai, 2004; Saito et al., 2009) and enzymatic pretreatments (Henriksson et al., 2007; Janardhnan & Sain, 2006; Pääkkö et al., 2007; Siddiqui, Mills, Gardner, & Bousfield, 2011; Zhu et al., 2011) have been employed to facilitate the disintegration of cellulose into nanofibrils and thus reduce energy consumption. A common chemical treatment involving 2,2,6,6-tetramethylpiperidinyl-1-oxyl (TEMPO) oxidation generated interfibrillar repulsive forces between fibrils by the conversion of primary hydroxyls in cellulose into carboxylate groups, which contribute to an easy and fast fibrillation (Saito et al., 2009; Siró & Plackett, 2010). Henriksson et al. (2007) proposed that endoglucanase treatment of softwood pulp fibers made it possible to create CNFs using a microfluidizer. Zhu, Sabo, and Luo (2011) showed that extensive enzymatic treatment of cellulose fibers yielded both sugar streams (for production of fuels and chemicals) and hydrolyzed cellulose fibers, and that the enzymatic treatment facilitated the production of CNFs. Such integrated approaches may be of importance to future biorefineries which might produce a multitude of varied product streams, including cellulosic nanomaterials, fuels and chemicals. Due to their environment friendliness, enzymatic pretreatment seems to be a promising approach for industrial applications (Engström, Ek, & Henriksson, 2006; Lavoine, Desloges, Dufresne, & Bras, 2012).

Despite all the studies describing CNFs, the effect of pretreatments and mechanical disintegration processes on the morphology and properties of cellulose nanofibrils is still not clear. For example, Siddiqui et al. (2011) concluded that enzyme pretreatment did not have a significant effect on the nanofibril size distribution, although they only measured the diameters of the fibers and did not show any comparative images of the CNFs prepared under different conditions. However, enzymatic treatments are known to affect fiber morphology, and we demonstrate such effects in this work. Here, we aim to further understand the effects of pretreatments and mechanical defibrillations on the properties of nanofibrils and films made from them. Grinding and high-shear homogenization, combined with chemical or extensive enzymatic pretreatment, are applied to produce various nanofibrils. The morphology and crystallinity of the cellulose nanofibrils, as well as mechanical and optical properties of their neat films are reported and compared.

2. Experimental

2.1. Materials

Commercially supplied bleached eucalyptus Kraft pulp (Aracruz Cellulose, Brazil) was received in dry form and used for the raw materials. After soaking in distilled water for at least 24 h, the pulp was disintegrated by shear mixing in a blender for 10 min. The mixture of pulp fiber and water were centrifuged and concentrated to 1.5 wt% consistency, which were employed in the subsequent pretreatments or mechanical disintegrations.

2.2. Preparation of cellulose nanofibrils

2.2.1. Enzyme pretreatment

The disintegrated eucalyptus pulp fibers were enzymatically pretreated using two formulations before mechanical fibrillation. The first enzyme formulation was simply a commercial grade endoglucanase of FiberCare® from Novozymes (Franklinton, NC). The second enzyme formulation was a mixture of FiberCare® and another complex enzyme cocktail, Cellulclast 1.5 L from Novozymes. The enzyme loading for both pretreatments was 3 FPU/g fiber. However, in the multiplex enzyme pretreatment, the loadings for FiberCare® and Cellulclast 1.5 L were 2 and 1 FPU/g fiber, respectively. Fibers were separately mixed with each enzyme formulation at 10% solids and incubated in a 1-L flask on a shaker (Thermo Fisher Scientific, Model 4450, Waltham, MA) at 50 °C and 200 rpm for 24 h. The resultant solids after enzymatic pretreatment were washed and then used for mechanical fibrillation.

Table 1
Preparation approaches for various cellulose nanofibrils.

Materials	Preparation approach		
	Pretreatment	Refining	Microfluidization
Pulp fiber	No	No	No
R	No	Yes	No
RM	No	Yes	Yes
ER	Enzyme	Yes	No
ERM	Enzyme	Yes	Yes
TEMPO	TEMPO	Yes	Yes

2.2.2. Mechanical fibrillation by the SuperMassCollider

The pulp fibers with or without enzymatic treatment were mechanically fibrillated at initial solids loading of 1.5% (w/w) using a MKZA6-2 SuperMassColloider (Masuko Sangyo Co. Ltd, Saitama, Japan) at 1500 rpm as described previously (Wang, Zhu, Gleisner, et al., 2012). The SuperMassCollider is equipped with two stone grinding disks (Disk Model: MKGA6-80#) and positioned on top of each other. The bottom disk rotates while the top disk is stationary. Pulp fiber suspension was fed into the disk grinder continuously by gravity using a loop consisting of a peristaltic pump (Cole Parmer, Chicago, IL) and plastic tubing. The gap of the two disks was adjusted to −100 μm from motion zero position after pulp fibers were loaded. The motion zero position was determined right at the contact position between the two grinding disks before loading pulp fibers. Due to the presence of pulp fibers, there was no direct contact between the two grinding stones even at a negative setting of disk position. Approximately 100 g pulp fibers (on a dry basis) were ground for 6 h before use.

2.2.3. TEMPO oxidization

TEMPO-oxidized cellulose nanofibrils used in this study were prepared according to the work reported by Saito et al. (2009). The same bleached eucalyptus pulp fibers were carboxylated using 2,2,6,6-tetramethylpiperidine-1-oxyl (TEMPO), sodium chlorite, and sodium hypochlorite as the reactants at 60 °C for 48 h. TEMPO oxidized pulp fibers were then washed thoroughly using distilled water and homogenized in a disk refiner to break apart fibril bundles. The fiber slurry was diluted to facilitate separation of coarse and fine fractions by centrifugation at 12,000 × *g*, and the coarse fraction was rejected. The nanofiber suspension was concentrated to a solid content of approximately 0.4% using ultrafiltration. A final clarification step was performed, in which the nanofiber suspension was passed once through an M-110EH-30 microfluidizer (Microfluidics, Newton, MA) with 200- and 87-μm chambers in series. The carboxylate content of reacted pulp fibers was measured via titration based on TAPPI Test Method T237cm-98 and found to be 0.46 mmol COONa per gram of pulp.

2.2.4. Microfluidization

A portion of the pulp refined for 6 h in the SuperMassCollider was further refined in the microfluidizer. The refined pulp fiber suspensions were diluted to 1% solids consistency and passed through the 87 μm chamber of the microfluidizer 15 times. The pressure of the acting chamber was adjusted to 150 MPa.

All cellulose nanofiber suspensions were stored in 4 °C room until further characterization or processing into films. The samples were given label designations of R, RM, ER, ERM, TEMPO (seen in Table 1), where "R" and "M" correspond to mechanical fibrillations of refining in the SuperMassColloider and microfluidizer,

respectively. The designations of "E" and "TEMPO" are pretreatments of enzyme and TEMPO oxidation, respectively. The detailed information for different processing methods is shown in Table 1.

2.3. Preparation of CNF films

The CNF films were prepared by filtering CNF suspensions, followed by air- and oven-dried drying the wet films. The nanofiber solutions, which were diluted to 0.2% solids concentration, were filtered using a 142 mm diameter Millipore ultrafiltration system (Millipore, Millipore Corporation, USA) under 0.55 MPa air pressure. Omnipore™ filter membranes with a pore size of 0.1 μm (JVWP14225, JV, Millipore Corporation, USA) were used in the apparatus and were supported by filter paper. The wet films were peeled from the membrane and stacked first between waxy coated papers and blotting papers. This assembly was maintained in between two metal plates and was air dried at room temperature for 24 h and then oven dried at 60 °C for 8 h under a load of approximately 250 N. The films were then conditioned in a 50% relative humidity chamber at a temperature of 23 °C until tested.

2.4. Characterization of cellulose nanofibrils

2.4.1. Morphology

The morphology of different cellulose nanofibrils was observed by scanning electron microscopy (SEM) and transmission electron microscopy (TEM). For preparation of SEM samples, a drop of diluted CNF suspension (with solid consistency of 0.005%) was directly placed on the well-polished aluminum SEM stubs and dried for 24 h at room temperature. In order to improve conductivity, the samples were sputtered with thin gold layer. The images were observed and recorded using a Zeiss EVO40 SEM (Carl Zeiss SMT Inc., Thornwood, NY, USA).

For TEM imaging, a diluted CNF suspension was deposited to a glow-discharged copper grid with formvar and carbon film (400 mesh). The droplet was maintained on the grid for 2 min, and then rinsed thoroughly using a 2% aqueous uranyl acetate stain followed by blotting. Samples were imaged using a Philips CM-100 TEM (Philips/FEI Corporation, Eindhoven, Holland) which operated at 100 kV, spot 3200 μm condenser aperture and 70 μm objective aperture. The images were captured and recorded using a SIA L3C 4-2Mpixel CCD camera (Scientific Instruments and Application, Duluth, GA, USA).

The diameter for different CNFs were measured and calculated on the basis of TEM images using the GNU Image Manipulation Program (GIMP, free download from http://www.gimp.org/) software. A minimum of 50 measurements were made to evaluate the fiber diameter for at least 5 images under each condition.

2.4.2. Degree of polymerization (DP)

The degree of polymerization (DP) for each CNF suspension was estimated based on the intrinsic viscosity. Measurements of viscosity for resulting CNF suspension was carried on according to TAPPI Standard Method T230 om-99 at 1% solid consistency, using 0.5 M cupriethylenediamine (CED) as dissolving agent and a capillary viscometer. DP value were then calculated by the following equation: $DP = 120 \times [\eta]^{1.11}$, where η is the viscosity (Alexander, Goldschmid, & Mitchell, 1957).

2.4.3. Crystallinity

The X-ray diffraction (XRD) patterns for different CNFs were measured with a Bruker/Siemens Hi-Star 2d Diffractometer (Bruker AXS, Madison, WI, USA) using Cu Kα radiation generated at 40 kV and 30 mA. The dried neat CNF films were individually mounted in a special holder through which X-ray beam centrally passed. Scattering radiation was detected in a 2θ range from 2° to 40° at a scanning rate of 4°/min. The crystallinity index (CI) was calculated from the XRD patterns followed the equation $CI = [(I_{200} - I_{am})/I_{200}] \times 100\%$ in accordance to the Segal method (Segal, Creely, Martin, & Conrad, 1959). Where I_{200} is the intensity height of crystalline (2 0 0) peak (at $2\theta = 22.5°$), I_{am} is the minimum intensity height between (2 0 0) and (1 0 1) peaks (at $2\theta = 16.3°$).

Table 2
DP and crystallinity of various cellulose nanofibrils. The "XRD" and "Raman" indicate crystallinity calculated from X-ray and Raman spectroscopy, respectively. "-" means not measured.

Materials	Main characteristic		
	DP	$Crystallinity_{XRD}$ (%)	$Crystallinity_{Raman}$ (%)
Pulp fiber	1000	55	–
R	836	47	38
RM	664	44	39
ER	287	60	44
ERM	263	57	43
TEMPO	580	34	25

Univariate Raman crystallinities of the samples were estimated using the previously established method (Agarwal, Reiner, & Ralph, 2010, 2012), The Raman method is based on the ratio of the cellulose peak heights at 380 and 1098 cm^{-1} in the spectrum of a sample and has shown good correlation with the XRD methods. Hemicellulose was present in only a small amount, so the crystallinities reported in Table 2 were not corrected for hemicellulose. Raman spectra of the sample pellets were obtained with a MultiRam spectrometer (Bruker Instruments Inc., Billerica, MA, USA). The laser power used for sample excitation was about 600 mW, and 1024 scans were accumulated. Bruker's OPUS software program was used to find peak positions and process the data. Processing of the spectra included, among other things, selecting a specific region, baseline correction, and normalization.

2.5. Characterization of CNF films

2.5.1. Tensile test

The tensile properties of different CNF films were tested by an Instron 5865 universal material testing apparatus (Instron Engineering Corporation, MA, USA) with a 500 N load cell, according to ASTM D638-10. The specimens were cut to conform to ASTM D638-10 type V dog bone shape using a special die (Qualitest, FL, USA) and were subsequently conditioned at 50% RH and 23 °C for at least 1 week prior to testing in a room, which was also conditioned at 50% RH and 23 °C. The specimens were pre-loaded with 5 N of force to remove slack, and the tests were performed with a crosshead speed of 1 mm/min. At least 6 specimens were tested for each condition. An LX 500 laser extensometer (MTS Systems Corporation, MN, USA) was used to determine the displacement with sampling frequency of 10 Hz. The laser recorded the displacement between two strips of reflective tape initially placed approximately 8 mm apart on the necked-down region of the dog-bone specimens. Strain was calculated from the determined displacement and initial gage length. Tensile modulus was calculated as the slope of the stress–strain curve in the stress region of 30–70 MPa. Film densities were calculated gravimetrically by measuring the dimensions and weight of multiple well-defined sections of each film. The corresponding porosity was estimated as the following Eq. (1):

$$\text{Porosity}\,(\%) = \left(1 - \frac{\rho_{fil}}{\rho_{cell}}\right) \times 100 \quad (1)$$

Here ρ_{fil} and ρ_{cell} represent density of the obtained CNF films and neat cellulose (1500 kg/m^3), respectively.

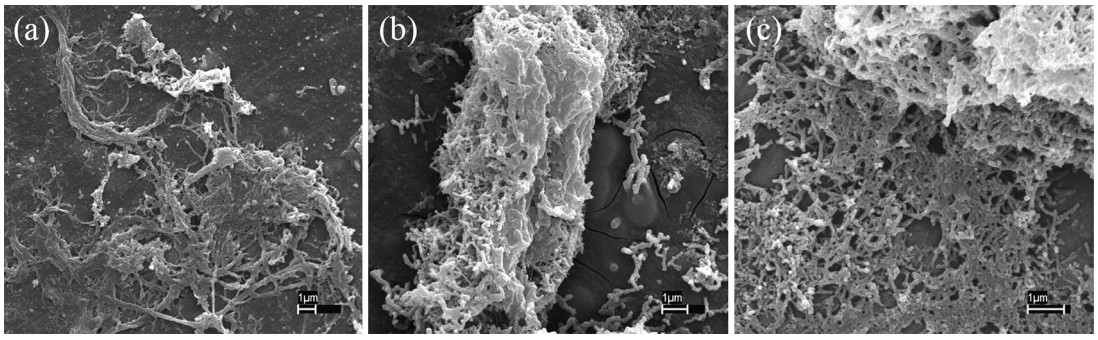

Fig. 1. SEM images of different cellulose nanofibrils; a, b, and c represent R, ER and ERM ones, respectively. The scale bar is 1 μm.

2.5.2. UV–vis light transmittance

The visible light transmittance for different CNF films were measured at a wavelength range from 400 to 800 nm by using a U-4100 ultraviolet-visible (UV–vis) spectrometer (Hitachi High Technologies America Inc., IL, USA). Rectangular specimen with size of 40 mm × 9 mm (length × width) were placed in a quartz cuvette and measured by placing it 25 cm from the entrance port of the integrating sphere. The specimens were conditioned at 50% RH and 23 °C for 2 days, and two tests were performed for each sample.

3. Results and discussion

Significant differences among the properties of the various CNFs and their films were found. The type of pretreatment (chemical or enzymatic), as well as the type of mechanical disintegration resulted in nanofibrils and films with varying characteristics. However, there was little difference between the effect of single and multiple enzyme treated CNFs in terms of the fiber or film properties. Therefore, for ease of discussion, only the results of single enzyme treated CNFs are provided.

3.1. Properties of cellulose nanofibrils

3.1.1. Morphological characteristics

Figs. 1 and 2 show SEM and TEM images, respectively, of the cellulose refined under various conditions. The original pulp fibers had an average diameter of about 18 μm and length of nearly 1 mm. As indicated in Fig. 1a, refining with the SuperMassColloider alone was not sufficient to completely reduce the cellulose fibers to nanofibrils, which produced nanofibers with diameters in the range of 9.0–170 nm and having an average diameter of 48 ± 45 nm as measured from TEM images. Larger, micrometer-scale bundles were also observed by SEM (Fig. 1a). However, it is worth noting that a significant portion of the fibers were converted to nano-scale fibers, which is consistent with previous results (Wang, Zhu, Gleisner, et al., 2012) for hardwood pulp refined using the same grinder. Refining in conjunction with the microfluidizer appeared to result in finer fibril structures than refining alone, and the fibril structures are highly networked (Fig. 2c). Diameters of RM nanofibrils were 4.7–31 nm with an average diameter of 15 ± 6.2 nm. In addition, this "RM" sample clearly had non-uniform fiber diameters with a large amount of "fuzzy" edges, unlike samples that had been pretreated with enzymes (Figs. 1b and c, and 2a and b). The diameters of the fibers appear to be decreased after passing through microfluidizer, which is consistent with previously reported results in which fiber bundles as a result of refining were converted into more uniform nanofibrils by high-pressure homogenization (Stelte & Sanadi, 2009).

Enzymes had a significant effect on the morphology of the CNFs. Large portions of short, rod-like particles can be seen in SEM and TEM (Figs. 1 and 2) images of the enzyme-treated fibers as compared to the larger, more networked nanofibrils created from mechanical refining alone. Enzymatically treated fibers subjected to microfluidizing had smaller diameters than those without microfluidizer treatment, which reduced the fiber diameter from a range of 16–87 nm and an average of 38 ± 21 nm to a range of 7.5–17 nm with an average of 12 ± 2.4 nm. Furthermore, the fiber diameters for fibers subjected to both microfluidizing and grinding had similar diameters whether treated with enzymes or not (Fig. 1), which is similar to the results presented by Siddiqui et al. (2011). However, not only do the enzymes reduce the length of course pulp fibers (Zhu et al., 2011), but the enzyme-treated fibers qualitatively appear to be shorter or at least less networked and more individualized than those without enzyme treatment. These fibers subjected to enzymatic pretreatment and high levels of mechanical refining appear to look similar to cellulose nanocrystals (CNCs) created by strong acid hydrolysis and shown elsewhere (Habibi, Lucia, & Rojas, 2010; Liu, Liu, Yao, & Wu, 2010; Wang, Zhu, Reiner, et al., 2012). Though similar to CNC in morphology, "ERM" nanofibrils differed from CNCs as discussed in a later section. Additionally, the enzymatic hydrolysis also facilitated processing in the microfluidizer by reducing the amount of clogging that occurred, which is consistent with previous reports (Henriksson et al., 2007). In the present study, extensive enzymatic hydrolysis was carried out in part to evaluate the properties of CNFs as part of an integrated biorefinery approach (Zhu et al., 2011). The morphology of the resulting material is much different from the mild to moderate enzymatic hydrolysis in which highly networked fibers remained (Henriksson et al., 2007; Pääkkö et al., 2007).

A simplified representation of the morphological observations of the conversion of cellulose in CNFs is that: (1) enzymatic treatment led to reduced length and reduced networking of fibers; (2) refining in a SuperMassCollider grinder resulted in non-uniform fibril bundles; and (3) the high-pressure microfluidizer resulted in a further liberation of the bundles into more uniform fibrils. Clearly, the mechanisms of these refining methods are different and result in different fibril morphology. Although the type of refining process of SuperMassCollider grinder is more readily scalable and industrially preferred, its implementation in the manner studied here suggests apparent limitations in the ability to fully create highly uniform nanomaterials, although Wang, Zhu, Gleisner, et al. (2012) previously demonstrated that some fraction of the fibrillated material is truly nano-scale. Furthermore, multi-staged or optimization of process conditions (e.g., temperature, solids content, disk gap) may result in more uniform fibers or tailored nanofibril morphologies. However, processing the cellulose to a homogeneous, nano-scale material may not be necessary depending on the application and desired properties of the CNFs.

As a comparison, Fig. 2d shows the morphology of CNFs from TEMPO-oxidation under neutral conditions. The introduction of negative carboxyl groups on nanofibril surface generates strong repulsive force which resulted in separated individual nanofibrils

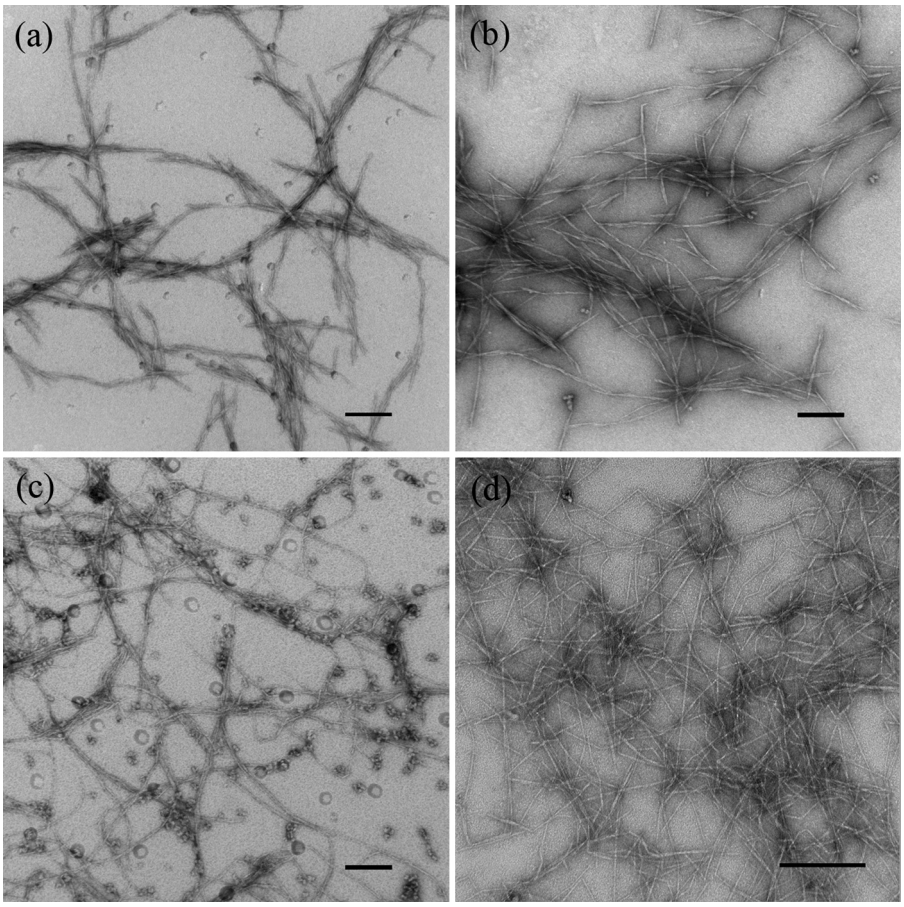

Fig. 2. TEM images of different cellulose nanofibrils; a, b, c and d represent ER, ERM, RM and TEMPO ones, respectively. The scale bar is 200 nm.

with narrow diameter distribution of (Saito et al., 2009). TEMPO oxidized CNFs had highly uniform diameters in the range of 5–7 nm (5.7 ± 0.7 nm average diameter) with length of more than several micrometers.

3.1.2. Degree of polymerization

Degree of polymerization (DP) is an important parameter for evaluating the length and branching of cellulose chains and is frequently used to the assessing of CNF products (Herrick et al., 1983; Saito et al., 2009; Zimmermann et al., 2010). Shinoda, Saito, Okita, and Isogai (2012) demonstrated that the fiber length of TEMPO-oxidized nanofibers linearly correlated with the DP value. Since the mechanical properties of CNF-based materials are strongly dependent on fiber length (Henriksson, Berglund, Isaksson, Lindström, & Nishino, 2008), evaluation of DP could provide valuable information about subsequent comparisons of CNF films.

Table 2 gives the DP value for the various CNFs prepared in this study. The DP of original pulp fiber is approximately 1000. Extensive refining in the SuperMassCollider grinder reduced the DP to 836, and further microfluidization caused the DP to decrease to 664. The further reduction in DP by microfluidization is considered to result from the liberation of large bundles of microfibrils. Enzymatic treatment clearly had the largest impact on DP with the DP of enzymatically pre-treated CNFs being reduced below 300. This significant reduction in DP is consistent with the reduced nanofiber lengths observed and previously mentioned. Here, the DP of TEMPO-oxidized CNFs was measured to be 580. Saito et al. (2009) reported that the TEMPO-oxidation did not significantly degrade initial structural properties of cellulose fibrils, depending on the reaction condition and time with a maximum of about 30% reduction in DP after nearly 60 h of reaction. In our study, the DP was reduced by more than 40% after 48 h despite the degree of substitution of carboxylate groups only about 60% as high as achieved by Saito et al. (2009). Regardless, the results showed that chemical, mechanical, and enzymatic treatments produced CNFs with reduced DP.

3.1.3. Crystallinity change

The XRD patterns for original pulp fiber and CNFs prepared by different approaches are shown in Fig. 3. Because there was little difference between XRD graphs of similar CNFs, such as R and

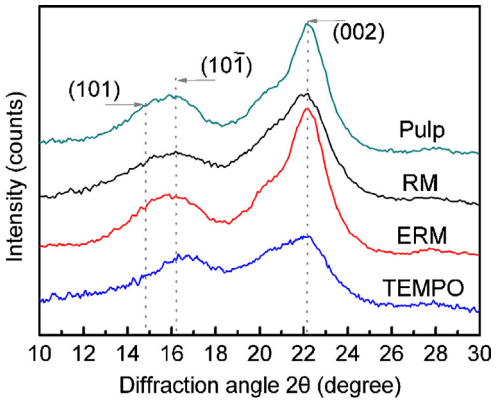

Fig. 3. XRD patterns for pulp fiber and different cellulose nanofibrils.

RM, only the diffractograms of RM and ERM are shown here along with those for the original pulp and TEMPO-oxidized CNFs. All the samples exhibited a sharp peak at $2\theta = 22.3^\circ$, suggesting the fibers contain a significant portion of native cellulose I since the characteristic peak at 22.6° corresponds the (0 0 2) lattice plane of cellulose I (Besbes, Alila, & Boufi, 2011; Tonoli et al., 2012). In addition, the overlapping peak of (1 0 1) and ($10\bar{1}$) lattice planes, which are characterized at $2\theta = 14.8^\circ$ and 16.3°, respectively, is prominently shown in the patterns. Therefore, the methods, including TEMPO-oxidation, for producing CNFs in this work did not alter the crystal structure. Similar results were found in previous studies (Saito et al., 2009; Tonoli et al., 2012; Wang, Zhu, Gleisner, et al., 2012). Although the crystal structure was not altered, the intensity of diffraction peaks varied significantly among the samples. The crystallinity index for the various samples is given in Table 2. In addition to XRD, Raman spectroscopy was used to estimate crystallinity and the results are reported in Table 2. In Raman, the crystallinity calculation is based on the ratio of the peak heights, 380–1098 cm^{-1} (Agarwal et al., 2010, 2012). A comparison of the spectra of the samples indicated that cellulose I was present in all samples.

Mechanical fibrillation by refining and microfluidization both appear to indiscriminately break apart crystalline and amorphous region of cellulose, resulting in decrease in crystallinity for the R and RM nanofibers. This breakage of cellulose crystals is believed to contribute the separation of microfibrils and its bundles (Wang, Zhu, Gleisner, et al., 2012; Zimmermann et al., 2010). Interestingly, the XRD crystallinity for nanofiber pretreated by enzyme hydrolysis increased to 60% compared with a pulp fiber crystallinity of 55%. In Raman though, the increase was lower (6% compared to 13% in XRD, Table 2). The increase of crystallinity confirms above hypothesis that the enzyme selected partially digests amorphous regions. This is consistent with the morphological observation that enzymatically pretreated nanofibers mostly look like rod-shaped cellulose crystals or whiskers (Figs. 1 and 2), which have higher crystallinity due to removal of amorphous cellulose by strong acid (Li et al., 2009; Liu et al., 2010). The TEMPO-oxidized nanofiber is calculated having relative low crystallinity of 34% by XRD and 25% by Raman. The TEMPO-oxidized CNFs were subjected to a high level of refining and one pass through the microfluidizer, and previous reports showed that high level homogenization dramatically reduced the crystallinity of TEMPO-oxidized nanofibrils (Besbes et al., 2011). Other methods, such as fibrillation using strong ultra-sonication, were observed to decrease the XRD crystallinity of eucalyptus nanofibrils to 33% (Tonoli et al., 2012). Although the procedure for mechanical refining of TEMPO and other samples was not exactly the same, it seems unlikely that mechanical refining alone was responsible for the crystallinity of TEMPO CNFs being lower than other CNFs in this study.

3.2. Characteristic of CNF films

3.2.1. Density and porosity

Density is an important indictor of the mechanical strength neat CNF films of polymer based composites (Henriksson et al., 2008; Takagi & Asano, 2008). It is supposed that, due to more condense structure and tighter fiber contact, higher density would result in higher mechanical strength. Furthermore, the density of cellulose nanofiber film has also been shown to be related to the diameter of raw nanofibers, which in turn indicates levels of fibrillation (Spence et al., 2011).

Fig. 4 shows the density and porosity of CNF films prepared from different nanofibrils. The density is estimated gravimetrically based on the weight and volume of dog bone specimens. Such methods tend to produce higher results than those measured by immersing samples into mercury (Henriksson et al., 2008). Generally speaking,

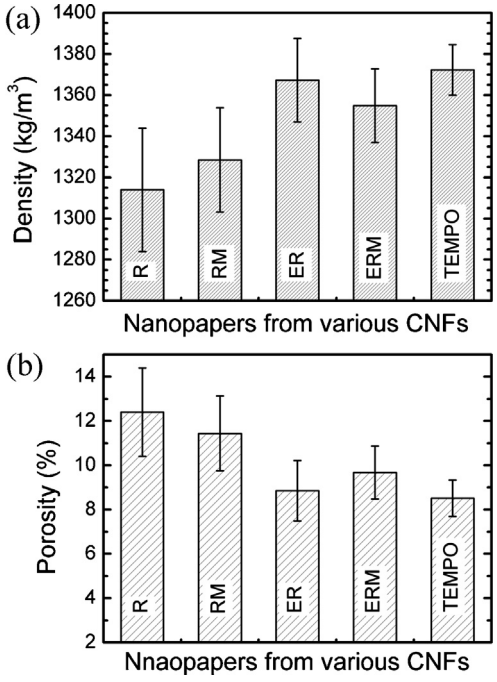

Fig. 4. Density (a) and porosity (b) of CNF films prepared from different nanofibrils.

CNFs with smaller diameters resulted in films with higher density, indicating a structure with better packing. Accordingly, the porosity is reduced gradually with decreasing fibril diameter. However, the films prepared from ER and TEMPO-oxidized nanofibrils had comparable density. This is due to the enzymatic hydrolysis, which partially removed the disorder regions of cellulose while mostly preserving the crystalline region having dense structure (Nelson & O'connor, 1964). However, the density of films measured is within the range of those reported elsewhere (Henriksson et al., 2008; Saito et al., 2009).

3.2.2. Mechanical properties

Although there are a few studies in which tools such as atomic force microscopy (AFM) are used to measure the mechanical properties of single CNFs (Cheng & Wang, 2008; Iwamoto, Kai, Isogai, & Iwata, 2009), such procedures are difficult and tedious and may not accurately represent the entire sample. Therefore, to gauge the mechanical properties of CNFs, films are typically formed and tested as an indirect evaluation of the mechanical properties of the CNFs. However, one should be cautioned from inferring the mechanical strength of individual fibrils or fibers from the results of such mechanical testing. Nonetheless, tensile testing of films can provide some insight into the nature of the materials.

The maximum tensile stress of films prepared from different CNFs is shown in Fig. 5a. It can be seen the TEMPO films had highest mechanical strength of approximately 220 MPa, which is consistent with our previous results (Qing et al., 2012, 2013) and is in the range of similar CNFs (Siró & Plackett, 2010). However, Saito et al. (2009) reported tensile strength of 312 MPa for CNF films prepared using the procedure on which the preparation of TEMPO-oxidized CNFs from this study was based. It should be noted the DP of the CNFs in that study was significantly higher than in the present study. Films made from enzymatic pretreated CNFs have relatively low maximum tensile stress of approximately 120 MPa. Furthermore, the result from analysis of variance (ANOVA) shows there is little difference in stress between ER and ERM films. Likely, the short and stiff CNC-like enzymatically pretreated nanofibrils did not have an interconnected network, which is beneficial for

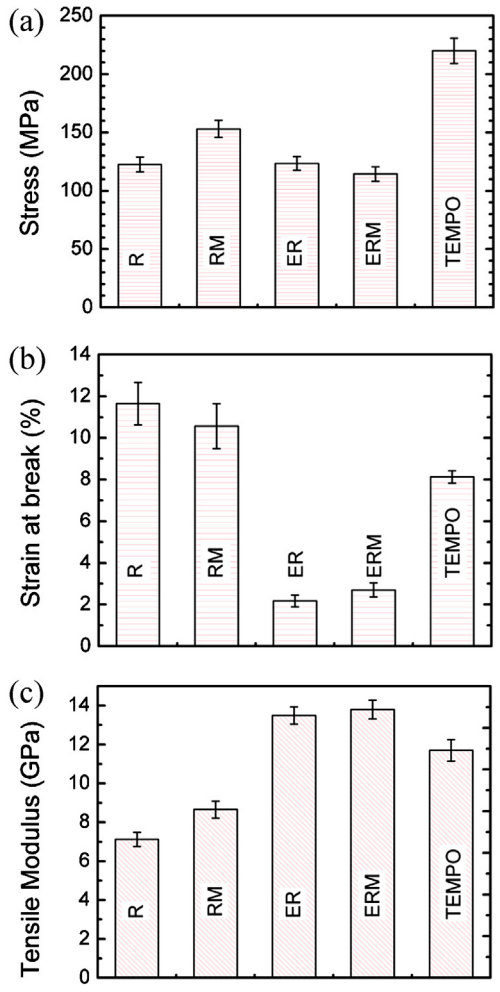

Fig. 5. Main tensile properties of CNF films prepared from various cellulose nanofibrils. (a) Stress; (b) Strain at break; (c) Tensile modulus.

enhancement of toughness (Henriksson et al., 2008). In addition, the increased defects among fiber ends caused by short rod-liked nanofibrils could also result in a reduction of tensile strength (Stelte & Sanadi, 2009). The RM films had tensile strength of approximately 153 MPa and appear to be stronger than the R films. Further separation of microfibril bundles may improve the mechanical strength by reducing the defects generated among large fibers. Additionally, the increase of flexibility for RM nanofibrils is believed to enhance the network arrangement, which is efficient for stress transfer and distribution. It seems that uniform nanofibrils like TEMPO and RM with high aspect ratio (length/width) result in higher mechanical strength films due to more interfibril hydrogen bonding and network structure.

The strain at break for the various CNF films is shown in Fig. 5b. The high strain at break for films R and RM are likely due to their long, networked fibers, which is also consistent with a high DP. Henriksson et al. (2008) reported nanofibrils with higher DP accordingly resulted in increased strain at break. Fukuzumi, Saito, and Isogai (2012) also reported longer TEMPO-oxidized nanofibrils having higher DP contributed to increased strain at break. In their study, the higher strain usually was associated with higher tensile stress, which is different from the results here. However, the mechanisms for creating different CNFs result in drastically different morphologies.

The tensile modulus of the various CNF films is shown in Fig. 5c. Because the tensile modulus is calculated based on the initial linear region of the stress–strain curve, the deformation is elastic and

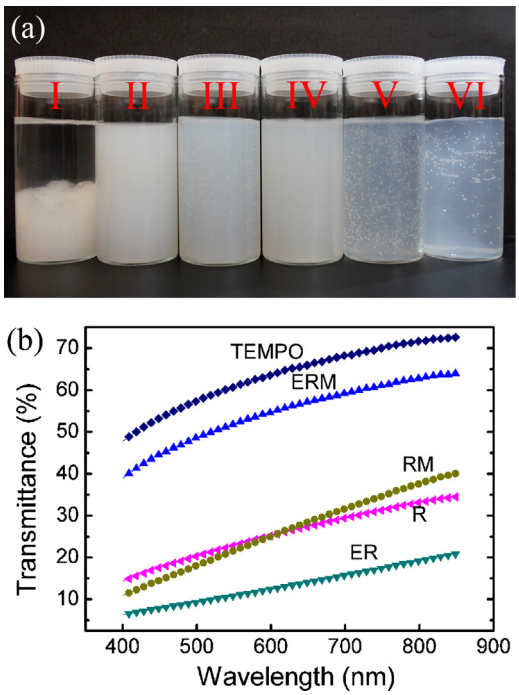

Fig. 6. Visual appearance of different CNF and pulp fiber suspensions (a) and UV–vis light transmittance of films from various CNFs. I: pulp fiber; II: R; III: RM; IV: ER; V: ERM; VI: TEMPO.

failure of individual nanofibrils is slight. As a consequence, elastic modulus strongly depends on the crystallinity of nanofibrils (Fukuzumi et al., 2012; Retegi et al., 2010) and on the density of nanopapers (Fukuzumi et al., 2012; Henriksson et al., 2008). Contrary to the stress and strain at break, the enzymatically pretreated nanofibrils had higher tensile moduli than the other samples. This is believed as a result of highly crystalline nanofibrils, which are also suspected to be good candidates for reinforcing polymer composites. Although the crystallinity of the TEMPO-oxidized CNFs is low, the high density of the films due to the narrow size distribution of the fiber diameters lends to create a high tensile modulus for TEMPO-oxidized nanofibrils.

3.3. Optical properties

3.3.1. UV–vis light transmittance

The appearance of pulp fiber suspensions and CNF gels (diluted at 0.5% solid consistency) generated from different fibrillation approaches is shown in Fig. 6a. Compared to the original pulp fiber, the nanofibrils at different fibrillations are translucent and well dispersed in water. This is the consequence of strong hydrogen bonding between water and more accessible hydroxyl groups resulting from microfibril liberation action (Pääkkö et al., 2007). The light transmittance of the CNF gels and films can provide insight into the level of fibrillation as small fibers result in less light scattering (Besbes et al., 2011). Indeed, visual observation of the samples in Fig. 6a reveals the TEMPO and ERM gels appear to be more transparent. The visible light transmittance at 400–850 nm wavelength for films prepared from different CNFs is shown in Fig. 6b. The films have thicknesses varied by less than 5%, thus the impact of sample thickness on transmittance was not considered. The most transparent film is made from TEMPO CNFs, followed by ERM ones, which is consistent with electron microscopy and visual observation of the gels. Despite evidence that the microfluidizer reduced the fibril size, there was little transmittance difference showed in R and RM films, which implies slight fibrillation effect. Perhaps flocs

of networked fibers resulted in increased light scattering for the RM sample. Since the fiber size distribution influences the transmittance of CNFs sheets and CNF-reinforced composites (Iwamoto, Abe, & Yano, 2008; Liu et al., 2010), TEMPO and ERM nanofibrils are promising candidates for use in transparent nanocomposites.

3.3.2. Birefringence

None of the CNFs, including the CNC-like ones, produced by extensive enzymatic and/or mechanical treatments in this work showed static or flow birefringence. The TEMPO CNF gels produced here showed static birefringence, which has been previously reported (Isogai, Saito, & Fukuzumi, 2011). The TEMPO CNFs are charged because of the carboxyl groups created on the cellulose by oxidation of the C6 primary hydroxyl groups (Saito et al., 2009). These carboxyl surface groups impart a surface charge, which has been measured as a zeta potential of −80 mV (Ishii, Saito, & Isogai, 2011), and along with the highly entangled network structure of the TEMPO CNFs, result in a stable ordered gel that shows birefringence. Enzymatic and mechanical treatments do not yield CNFs with charged groups as the hydrolysis results in cleavage of the β-1,4-D-glycosidic bonds (Asztalos, Daniels, & Sethi, 2012). The zeta potential of such cellulose has been reported as only about −10 mV (Stenstad, Andresen, Tanem, & Stenius, 2008), so the solutions are not stable and agglomerate at low concentrations. Gels are formed at higher concentrations, but no birefringence was observed in these CNF gels. Numerous attempts were made to manifest flow or static birefringence in the CNC-like CNFs by adjusting concentrations and separating various size fractions, but none was observed. The lack of birefringence of these CNFs is likely due to the morphology of the fibrils, which may have irregular surfaces preventing their ordering in a manner to produce birefringence. The polydispersity of these CNC-like CNFs may also contribute to the lack of birefringence. Furthermore, the fibrils will tend to agglomerate due to their lack of surface charge. Although the lack of surface charge seems a possible culprit in preventing birefringence, CNCs produced by hydrochloric acid hydrolysis also lack the charge to produce stable dispersions (Habibi, Chanzy, & Vignon, 2006) but have been reported to show flow birefringence (Araki, Wada, Kuga, & Okano, 1998). Clearly, more work is needed to understand the relationship among the morphology, surface chemistry and properties of these cellulose nanomaterials.

4. Conclusions

Cellulose nanofibrils were successfully prepared using combinations of refining by a SuperMassCollider grinder and a microfluidizer along with enzymatic or TEMPO-oxidation pretreatments. Furthermore, an evaluation of CNFs produced as part of an integrated biorefinery approach in which sugars are extracted after enzymatic hydrolysis of wood pulp was provided here and compared to other methods of producing CNFs. Refining in the SuperMassCollider grinder led to highly networked, non-uniform fiber bundles, and processing in the microfluidizer after refining resulted in fibril bundles being sheared apart, resulting in smaller and apparently more uniform fiber diameters. Enzymatic pretreatments resulted in CNFs with shorter fibril lengths and higher crystallinity index, although the diameters were not significantly altered by enzymatic pretreatment. The enzyme-pretreated nanofibrils appeared stiff and had rod-like shape with fiber length of several hundred nanometers and were remarkably similar to cellulose nanocrystals prepared by strong acid hydrolysis. The combination of chemical (TEMPO-oxidation) or enzymatic pretreatment with both refining and microfluidization resulted in gels and films with transparency higher than CNF samples without all combinations of refining. Films prepared from the highly crystalline enzymatically pre-treated CNFs had the highest tensile stiffness and lowest strain at break. Such fibers may offer better potential as the reinforcing phase in composites than other types of CNFs, such as refined only using a SuperMassCollider grinder despite the higher tensile strength of films prepared from CNFs refined only using grinder. Highly networked CNFs resulted in films with the highest toughness and are possibly suited for applications, such as laminates, in which toughness is desired. TEMPO-oxidized CNFs showed high strength, high toughness and high stiffness. However, depending on the application, the extensive chemical and mechanical refining necessary to create TEMPO-oxidized CNFs may not be the most desirable, especially considering the high viscosity of suspensions of TEMPO-oxidized CNFs. A wide range of properties can be achieved using various combinations and levels of treatment, and this study provides further insight into the properties of CNFs produced using various methods.

Acknowledgements

This project is supported in part by the Agriculture and Food Research Initiative Grant (no. 2011-67009-20056) from the USDA National Institute of Food and Agriculture, and the National “948” Project of China (no. 2009-4-51). Enormous gratitude is offered to Rick Reiner for preparing and supplying TEMPO-oxidized cellulose nanofibrils. The authors acknowledge Benjamin Treml for helping with tensile testing. Tom Kuster of the Forest Products Laboratory and Debby Sherman via Purdue University are kindly acknowledged for SEM and TEM imaging, respectively.

References

Agarwal, U. P., Reiner, R. S., & Ralph, S. A. (2010). Cellulose I crystallinity determination using FT-Raman spectroscopy: Univariate and multivariate methods. *Cellulose*, *17*(4), 721–733.

Agarwal, U. P., Reiner, R. S., & Ralph, S. A. (2012). Estimation of cellulose crystallinity of lignocelluloses using near-IR FT-Raman spectroscopy and comparison of Raman and Segal-WAXS methods. *Journal of Agricultural and Food Chemistry*, http://dx.doi.org/10.1021/jf304465k

Alemdar, A., & Sain, M. (2008). Isolation and characterization of nanofibers from agricultural residues—Wheat straw and soy hulls. *Bioresource Technology*, *99*(6), 1664–1671.

Alexander, W. J., Goldschmid, O. T. T. O., & Mitchell, R. L. (1957). Relation of intrinsic viscosity of cellulose chain length-degree of polymerization range below 400. *Industrial and Engineering Chemistry*, *49*(8), 1303–1306.

Araki, J., Wada, M., Kuga, S., & Okano, T. (1998). Flow properties of microcrystalline cellulose suspension prepared by acid treatment of native cellulose. *Colloids and Surfaces A: Physicochemical and Engineering Aspects*, *142*(1), 75–82.

Asztalos, A., Daniels, M., Sethi, A., Shen, T., Langan, P., Redondo, A., et al. (2012). A coarse-grained model for synergistic action of multiple enzymes on cellulose. *Biotechnology for Biofuels*, *5*, 55–69.

Aulin, C., Gällstedt, M., & Lindström, T. (2010). Oxygen and oil barrier properties of microfibrillated cellulose films and coatings. *Cellulose*, *17*(3), 559–574.

Besbes, I., Alila, S., & Boufi, S. (2011). Nanofibrillated cellulose from TEMPO-oxidized eucalyptus fibers: Effect of the carboxyl content. *Carbohydrate Polymers*, *84*(3), 975–983.

Chakraborty, A., Sain, M., & Kortschot, M. (2005). Cellulose microfibrils: A novel method of preparation using high shear refining and cryocrushing. *Holzforschung*, *59*(1), 102–107.

Chen, W., Yu, H., Liu, Y., Chen, P., Zhang, X., & Hai, Y. (2011). Individualization of cellulose nanofibers from wood using high-intensity ultrasonication combined with chemical pretreatments. *Carbohydrate Polymers*, *83*(4), 1804–1811.

Cheng, Q., & Wang, S. (2008). A method for testing the elastic modulus of single cellulose fibrils via atomic force. *Composites Part A: Applied Science and Manufacturing*, *39*(12), 1838–1843.

Cheng, Q., Wang, S., & Rials, T. G. (2009). Poly(vinyl alcohol) nanocomposites reinforced with cellulose fibrils isolated by high intensity ultrasonication. *Composites Part A: Applied Science and Manufacturing*, *40*(2), 218–224.

Czaja, W. K., Young, D. J., Kawecki, M., & Brown, R. M. (2007). The future prospects of microbial cellulose in biomedical applications. *Biomacromolecules*, *8*(1), 1–12.

Engström, A.-C., Ek, M., & Henriksson, G. (2006). Improved accessibility and reactivity of dissolving pulp for the viscose process: Pretreatment with monocomponent endoglucanase. *Biomacromolecules*, *7*(6), 2027–2031.

Fukuzumi, H., Saito, T., & Isogai, A. (2012). Influence of TEMPO-oxidized cellulose nanofibril length on film properties. *Carbohydrate Polymers*, http://dx.doi.org/10.1016/j.crrbpol.2012.04.069

Habibi, Y., Chanzy, H., & Vignon, M. R. (2006). TEMPO-mediated surface oxidization of cellulose whiskers. *Cellulose*, *13*(6), 679–687.
Habibi, Y., Lucia, L. A., & Rojas, O. J. (2010). Cellulose nanocrystals: Chemistry, self-assembly, and applications. *Chemical Reviews.*, *110*(6), 3479–3500.
Herrick, F. W., Casebier, R. L., Hamilton, J. K., & Sandberg, K. R. (1983). Microfibrillated cellulose: Morphology and accessibility. *Journal of Applied Polymer Science: Applied Polymer Symposium*, *37*(9), 797–813.
Henriksson, M., Henriksson, G., Berglund, L. A., & Lindström, T. (2007). An environmentally friendly method for enzyme-assisted preparation of microfibrillated cellulose (MFC) nanofibers. *European Polymer Journal*, *43*(8), 3434–3441.
Henriksson, M., Berglund, L. A., Isaksson, P., Lindström, T., & Nishino, T. (2008). Cellulose nanopaper structure of high toughness. *Biomacromolecules*, *9*(6), 1579–1585.
Ishii, D., Saito, T., & Isogai, A. (2011). Viscoelastic evaluation of average length of cellulose nanofibers prepared by TEMPO-mediated oxidation. *Biomacromolecules*, *12*(3), 548–550.
Isogai, A., Saito, T., & Fukuzumi, H. (2011). TEMPO-oxidized cellulose nanofibers. *Nanoscale*, *3*(1), 71–85.
Iwamoto, S., Nakagaito, A. N., & Yano, H. (2007). Nanofibrillation of pulp fibers for the processing of transparent nanocomposites. *Applied Physics A: Materials Science & Processing.*, *89*(2), 461–466.
Iwamoto, S., Abe, K., & Yano, H. (2008). The effect of hemicellulose on the wood pulp nanofibrillation and nanofiber network characteristics. *Biomacromolecules*, *9*(3), 1022–1026.
Iwamoto, S., Kai, W., Isogai, A., & Iwata, T. (2009). Elastic modulus of single cellulose microfibrils from tunicate measured by atomic force microscopy. *Biomacromolecules*, *10*(9), 2571–2576.
Janardhnan, S., & Sain, M. M. (2006). Isolation of cellulose microfibrils—An enzymatic approach. *Bioresources*, *1*(2), 176–188.
Lavoine, N., Desloges, I., Dufresne, A., & Bras, J. (2012). Microfibrillated cellulose—Its barrier properties and applications in cellulosic materials: A review. *Carbohydrate Polymers*, *90*(2), 735–764.
Li, R., Fei, J., Cai, Y., Li, Y., Feng, J., & Yao, J. (2009). Cellulose whiskers extracted from mulberry: A novel biomass production. *Carbohydrate Polymers*, *76*(1), 94–99.
Liu, H., Liu, D., Yao, F., & Wu, Q. (2010). Fabrication and properties of transparent polymethylmethacrylate/cellulose nanocrystals composites. *Bioresource Technology*, *101*(14), 5685–5692.
Microfluidics Corporation. (2012). *Microfluidics*. http://www.microfluidicscorp.com/index.php?option=com_content&view=article&id=49&Itemid=180
Nakagaito, A. N., & Yano, H. (2004). The effect of morphological changes from pulp fiber towards nano-scale fibrillated cellulose on the mechanical properties of high-strength plant fiber based composites. *Applied Physics A: Materials Science & Processing*, *78*(1), 547–552.
Nelson, M. L., & O'Connor, R. T. (1964). Relation of certain infrared bands to cellulose crystallinity and crystal lattice type. Part II. A new infrared ratio for estimation of crystallinity in celluloses I and II. *Journal of Applied Polymer Science*, *8*, 1325–1341.
Nyström, G., Mihranyan, A., Razaq, A., Lindström, T., Nyholm, L., & Strømme, M. (2010). A nanocellulose polypyrrole composite based on microfibrillated cellulose from wood. *The Journal of Physical Chemistry B*, *114*(12), 4178–4182.
Okahisa, Y., Yoshida, A., Miyaguchi, S., & Yano, H. (2009). Optically transparent wood-cellulose nanocomposite as a base substrate for flexible organic light-emitting diode displays. *Composites Science and Technology*, *69*(11–12), 1958–1961.
Olsson, R. T., Azizi Samir, M. A. S., Salazar-Alvarez, G., Belova, L., Ström, V., Berglund, L. A., et al. (2010). Making flexible magnetic aerogels and stiff magnetic nanopaper using cellulose nanofibrils as templates. *Nature Nanotechnology*, *5*(8), 584–588.
Pääkkö, M., Ankerfors, M., Kosonen, H., Nykänen, A., Ahola, S., Österberg, M., et al. (2007). Enzymatic hydrolysis combined with mechanical shearing and high pressure homogenization for nanoscale cellulose fibrils and strong gels. *Biomacromolecules*, *8*(6), 1934–1941.
Qing, Y., Sabo, R., Wu, Y., & Cai, Z. (2012). High-performance cellulose nanofibril composite films. *Bioresources*, *7*(3), 3064–3075.
Qing, Y., Sabo, R., Cai, Z., & Wu, Y. (2013). Resin impregnation of cellulose nanofibril films facilitated by water swelling. *Cellulose*, *20*(1), 303–313.
Retegi, A., Gabilondo, N., Peña, C., Zuluaga, R., Castro, C., Gañan, P., et al. (2010). Bacterial cellulose films with controlled microstructure-mechanical property relationship. *Cellulose*, *17*(3), 661–669.
Sabo, R., Seo, J. H., & Ma, Z. (2012). Cellulose nanofiber composite substrates for flexible electronics. In *TAPPI international conference on nanotechnology for renewable materials* Montreal, Quebec, Canada.
Saito, T., & Isogai, A. (2004). TEMPO-mediated oxidation of native cellulose. The effect of oxidation conditions on chemical and crystal structures of the water-insoluble fractions. *Biomacromolecules*, *5*(5), 1983–1989.
Saito, T., Hirota, M., Tamura, N., Kimura, S., Fukuzumi, H., Heux, L., et al. (2009). Individualization of nano-sized plant cellulose fibrils by direct surface carboxylation using TEMPO catalyst under neutral conditions. *Biomacromolecules*, *10*(7), 1992–1996.
Segal, L., Creely, J. J., Martin, A. E., Jr., & Conrad, C. M. (1959). An empirical method for estimating the degree of crystallinity of native cellulose using the X-ray diffractometer. *Textile Research Journal*, *29*(10), 786–794.
Sehaqui, H., Allais, M., Zhou, Q., & Berglund, L. A. (2011). Wood cellulose biocomposites with fibrous structure at micro- and nanoscale. *Composites Science and Technology*, *71*(3), 382–387.
Shinoda, R., Saito, T., Okita, Y., & Isogai, A. (2012). Relationship between length and degree of polymerization of TEMPO-oxidized cellulose nanofibrils. *Biomacromolecules*, *13*(3), 842–849.
Siddiqui, N., Mills, R. H., Gardner, D. J., & Bousfield, D. (2011). Production and characterization of cellulose nanofibers from wood pulps. *Journal of Adhesion Science and Technology*, *25*(6–7), 709–721.
Siró, I., & Plackett, D. (2010). Microfibrillated cellulose and new nanocomposites materials: A review. *Cellulose*, *17*(3), 459–494.
Spence, K. L., Venditti, R. A., Rojas, O. J., Habibi, Y., & Pawlak, J. J. (2011). A comparative study of energy consumption and physical properties of microfibrillated cellulose produced by different processing methods. *Cellulose*, *18*(4), 1097–1111.
Srithep, Y., Turng, L.-S., Sabo, R., & Clemons, C. (2012). Nanofibrillated cellulose (NFC) reinforced polyvinyl alcohol (PVOH) nanocomposites: Properties, solubility of carbon dioxide, and foaming. *Cellulose*, *19*(4), 1209–1223.
Stelte, W., & Sanadi, A. R. (2009). Preparation and characterization of cellulose nanofibers from two commercial hard wood and softwood pulps. *Industrial & Engineering Chemistry Research*, *48*(24), 11211–11219.
Stenstad, P., Andresen, M., Tanem, B. S., & Stenius, P. (2008). Chemical surface modifications of microfibrillated cellulose. *Cellulose*, *15*(1), 35–45.
Takagi, H., & Asano, A. (2008). Effects of processing conditions on flexural properties of cellulose nanofiber reinforced green composites. *Composites Part A: Applied Science and Manufacturing*, *39*(4), 685–689.
Tingaut, P., Zimmermann, T., & Lopez-Suevos, F. (2010). Synthesis and characterization of bionanocomposites with tunable properties from poly (lactic acid) and acetylated microfibrillated cellulose. *Biomacromolecules*, *11*(2), 464–545.
Tonoli, G. H. D., Teixeira, E. M., Corrêa, A. C., Marconcini, J. M., Caixeta, L. A., Pereira-da-Silva, M. A., et al. (2012). Cellulose micro/nanofibers from *Eucalyptus* kraft pulp: Preparation and properties. *Carbohydrate Polymers*, *89*(1), 80–88.
Turbak, A., Snyder, F. W., & Sandberg, K. R. (1983). Microfibrillated cellulose, a new cellulose product: Properties, uses, and commercial potential. *Journal of Applied Polymer Science: Applied Polymer Symposium*, *37*(9), 815–827.
Uetani, K., & Yano, H. (2011). Nanofibrillation of wood pulp using a high-speed blender. *Biomacromolecules*, *12*(2), 348–353.
Wang, B., & Sain, M. (2007). Dispersion of soybean stock-based nanofiber in plastic matrix. *Polymer International*, *56*(4), 538–546.
Wang, Q. Q., Zhu, J. Y., Gleisner, R., Kuster, T. A., Baxa, U., & McNeil, S. E. (2012). Morphological development of cellulose fibrils of a bleached eucalyptus pulp by mechanical fibrillation. *Cellulose*, *19*(5), 1631–1643.
Wang, Q. Q., Zhu, J. Y., Reiner, R. S., Verrill, S. P., Baxa, U., & McNeil, S. E. (2012). Approaching zero cellulose loss in cellulose nanocrystal (CNC) production: Recovery and characterization of cellulosic solid residues (CSR) and CNC. *Cellulose*, *19*(6), 2033–2047.
Zhu, J. Y., Sabo, R., & Luo, X. (2011). Integrated production of nano-fibrillated cellulose and biofuel (ethanol) by enzymatic fractionation of wood fibers. *Green Chemistry*, *13*(5), 1339–1344.
Zimmermann, T., Bordeanu, N., & Sturb, E. (2010). Properties of nanofibrillated cellulose from different raw materials and its reinforcement potential. *Carbohydrate Polymers*, *79*(4), 1086–1093.